Int. J. Electrochem. Sci., 15 **(2020)** 8012 – 8025, doi: 10.20964/2020.08.07

International Journal of
ELECTROCHEMICAL
SCIENCE
www.electrochemsci.org

Corrosion Behavior of Al-Cu-RE(Re= La, Ce) Alloy Joints in Alkaline Soil Extract

Fengjie Yan[1,2], *Xuegang Wang*[3], *Xingeng Li*[2], *Chengguo Wang*[1,*] , *Bo Jiang*[2]

[1] School of Materials Science and Engineering, Shandong University, Jinan 250061, China
[2] Material Laboratory of State Grid Corporation of China (Shandong), State Grid Shandong Electric Power Research Institute, Jinan 250001, China
[3] School of Materials Science and Engineering, Shandong Jianzhu University, Jinan 250101, China
[*]E-mail: sduwchg@163.com

Received: 7 April 2020 / *Accepted:* 20 May 2020 / *Published:* 10 July 2020

The corrosion behavior of metal inert-gas (MIG) welded Al-Cu-RE alloy joint in alkaline soil extract was studied by immersion corrosion test and electrochemical test. The microstructure, surface potential, corrosion morphology and corrosion products were analyzed by metallographic microscope, scanning Kelvin Probe (SKP), 3D optical profiler, scanning electron microscope (SEM) combined with energy dispersive spectrometry (EDS). The corrosion of the welded Al-Cu-RE alloy joint is mainly related to the difference of microstructure and surface potential in each region of the joint. The surface potential of the weld zone (WZ) was significantly lower than that of both the base metal (BM) and the heat affected zone (HAZ). The copper atom segregates near the fusion line (FL) and the noble second phase concentrates at the grain boundary of columnar crystal. As a result, the weld zone had the worst corrosion resistance with the most serious corrosion of the columnar crystal zone. The corrosion characteristics were pitting corrosion and local exfoliation corrosion. The corrosion products were mainly aluminum oxides and sulfides.

Keywords: Al-Cu-RE alloy; welded joints; electrochemical; SKP; pitting corrosion

1. INTRODUCTION

AlCuRE alloy was used as grounding materials in grounding engineering to replace galvanized steel and copper due to its high specific strength, excellent grounding conductivity, good resistance to soil corrosion, low cost and environmental friendliness [1-2]. At present, the main welding methods to join Al-Cu alloy were still Friction Stir Welding (FSW), Tungsten Inert Gas (TIG), Plasma Arc Welding

(PAW) and Metal Inert Gas (MIG) [3-4]. However, MIG is the favorable welding method to join AlCuRE alloy in grounding engineering owing to the construction efficiency and feasibility.

The performances of welded joints are very important for the application of metal materials in engineering. Many scholars and technicians have focused on the corrosion behavior of welded joints. In recent years, the microstructure, mechanical properties as well as corrosion behavior of Al-Cu alloy joints produced by friction welding and TIG welding were investigated widely [5-20]. Zhang et al. investigated the corrosion behavior of 2219 aluminum alloy welded joints and believed that the intergranular corrosion behavior of both base metal and welded joint were related to precipitation phase. The precipitation of Al_2Cu phase caused the dissolution of poor Cu zone as the anode, which first appeared pitting corrosion and finally developed into exfoliation corrosion. TIG welding joints showed intergranular corrosion with network cracks, and FSW showed pitting corrosion [3]. As it is known, segregation is the main factor to cause corrosion of high-strength aluminum alloys. According to the in-situ monitoring of friction welded AA2024-T3 joint, it was found that pitting corrosion originated from the S-phase particles and the adjacent aluminum base metal. The higher self-corrosion potential of these inter-metallic compounds can cause anodic dissolution of the surrounding aluminum substrate and then result in pitting corrosion[6,7,10]. Kang et al. found that the abnormal θ particle agglomerations resulted in more severe localized attack because of the large ratio of cathode/anode [12]. Some study has shown that post-weld heat treatment can change microstructure of the welded joint and then increase its stress corrosion resistance [15,16,21]. The dynamic polarization curve test has shown that the corrosion resistance of electron beam welded 2219 aluminum alloy joint is superior to that of the tungsten argon arc welded joint. The main reasons should be the fine equiaxed grain structures, homogenous distribution of copper and small pores of the electron beam welded joint [22]. Some scholars have studied the corrosion behavior of MIG welded A7N01S-T5 aluminum alloy joints through salt spray corrosion tests. The corrosion mechanism of the welded joint was pitting corrosion firstly and then came to denudation corrosion with the corrosion pit spreading into the inner of the joint. The grains of the heat affected zone (HAZ) zone were coarsened with the partially overheat during welding, and it was very sensitive in the salt fog corrosion test [23].

At present, there are few studies on the corrosion behavior of MIG welded Al-Cu alloys joints, especially on corrosion in soil extract. In this study, the corrosion behavior of MIG welded AlCuRE alloy joints in alkaline soil extract was studied by immersion test and electrochemical test in the laboratory.

2. EXPERIMENTAL

2.1. Material and welded joint

The base materials was AlCuRE alloy strip with a size of 60mm × 6mm× 300mm. MIG welding process was utilized to join these AlCuRE alloy strip. The filler material was ER4043 Al-Si welding wire with the diameter of 1.6mm. The chemical compositions of both base material and filler material were shown in Table 1. The MIG welding parameters were shown in Table 2. Before welding, an X-

shaped groove was required. The MIG welded joint includes weld zone (WZ), fusion line (FL) and heat affect zone (HAZ), as shown in Figure 1.

Samples for microstructure analysis, electrochemical experiment and immersing test were cut to 20mm×5mm×5mm from the zone of base metal and welded joints, respectively. The samples were firstly abraded with 400#, 600# and 1000# grit abrasive papers and polished with diamond polishing solution. The samples were cleaned ultrasonically using acetone and then rinsed using ethanol. An area of 1 cm^2 was exposed by covering other parts with epoxy resin. The metallographic samples were etched using Dix-keller's reagent and then investigated using an optical microscope (OM) and scanning electron microscope (SEM) combined and energy dispersive spectrometry (EDS) before corrosion test.

Table 1. Chemical compositions of AlCuRE base metal and ER4043 fill material (mass %).

	Elements (mass %)									
Alloy	Cu	Si	La	Ce	Mg	Fe	Zn	Mn	Others	Al
AlCuRE	4.61	0.02	0.12	0.08	-	0.10	-	-	-	Bal.
ER4043	0.04	5.00	-	-	0.10	0.04	0.10	0.04	0.10	Bal.

Table 2. MIG welding parameters.

Current/ A	Arc voltage / V	Welding speed/ $mm \cdot min^{-1}$	Argon flow / $L \cdot min^{-1}$
135~145	21	150~180	12

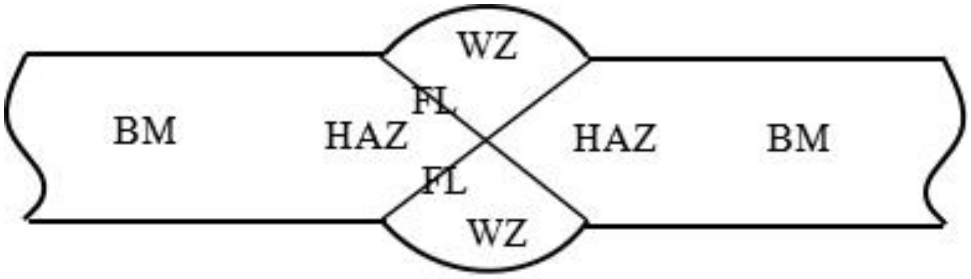

Figure 1. Schematic diagram of MIG (metal inert-gas) welded joint: HAZ (heat affected zone), FL (fusion line), WZ (weld zone), BM (base metal).

2.2. Corrosion medium

Corrosion medium was liquid soil extract. Some solid soil was dug in 0.8 meters deep underground. 20-mesh dry soil was prepared by grinding, sieving and 6 hours drying in an electric furnace. After 200g of dry soil were mixed with 1000ml deionized water by mechanical stirring, the liquid soil extract was produced by filtering out the mixture. The composition and some physical properties of the soil extract were shown in Table 3. It can be seen that the liquid soil extract is alkaline with pH>7.

Table 3. Composition (mass%) and physical properties of soil extract.

Ca^{2+}	Mg^{2+}	K^{+}	Na^{+}	Cl^{-}	SO_4^{2-}	NO_3^{-}	HCO_3^{-}
0.0415	0.0124	0.0046	0.1118	0.0918	0.0209	0.0052	0.2733

pH value(1:2.5)	Conductivity of soil extract（μS/cm 1:5）	Conductivity of filtered soil（μS/cm 1:2.5）
9.23	885	536

Note: 1:2.5 and 1:5 represent the mass ratio of the soil to the water.

2.3. Corrosion test

Electrochemical experiments were conducted in liquid soil extract by using a PARASTAT2273 electrochemical workstation with a three-electrode system. The three-electrode system involved working electrode(WE), reference electrode (RE) and counter electrode (CE), which were the welded joint, the saturated calomel electrode and the platinum plate electrode, respectively. Potentiodynamic polarization curves were gained at the range between -250 mV and 250 mV relative to open-circuit potential (OCP) by a 0.333 mVs^{-1} scanning rate. Electrochemical Impedance Spectroscopy (EIS) were measured between 100 kHz and 100 mHz under an amplitude signal of 10mV and then analyzed using ZSimpwin software. All the electrochemical test were carried out at room temperature.

Immersion test was performed in soil extract for 150 hours at room temperature. The surface potential of the samples were scanned with the Versascan micro-scanning electrochemical workstation by Scanning Kelvin Probe (SKP) test after being immersed for different time. The surface corrosion morphology of the sample was observed with an optical profiler after being immersed for different time. Both tests of SKP and 3D optical microscopy are non-contact surface measurements. All samples were taken out from the liquid soil extract when the immersion test was running for 150 hours. The corrosion products were tested by SEM and EDS after all samples were firstly cleaned using distilled water and then dehydrated with absolute ethanol.

SKP test was conducted in air at room temperature with the step scan mode for map scanning. The scanning step was 100μm, the scanning area was 10000μm × 3000μm. The average distance between the probe and the sample surface was about 100μm.

3. RESULTS AND DISCCUSION

3.1. Microstructure

The optical microstructures of MIG welded AlCuRE joint are shown in Fig.2. The microstructure of HAZ is a feature of the hot rolled structure. The microstructure of the WZ is the as-cast structure with equiaxed dendrite in the central of WZ and the columnar crystal near the FL. Since the cooling speed of the molten pool near the FL is faster than that in the center of the WZ, the columnar crystal structure appears near the FL.

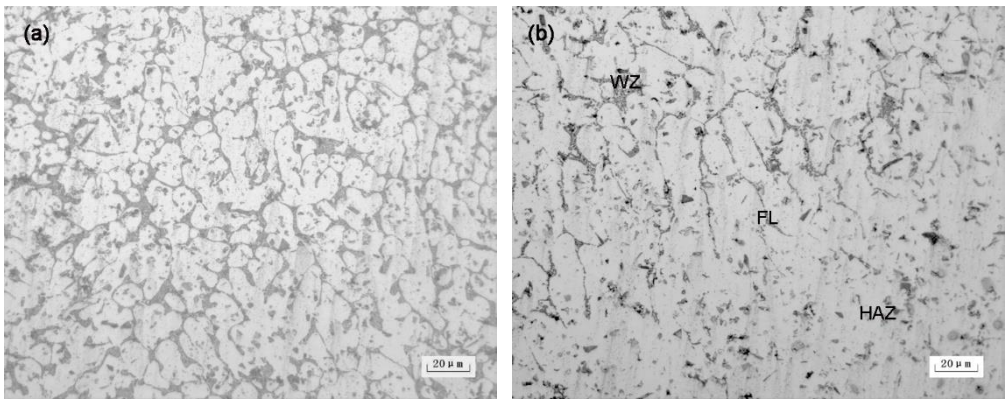

Figure 2. OM images of MIG welded AlCuRE alloy joint samples: (a) WZ, (b) welded joint near the FL.

Fig.3 shows the SEM microstructures of AlCuRE welded joint. It can be seen that there are many grain boundaries and dendrites in the weld zone from the backscattered electron micrographs of the joint around FL, as shown in Fig.3a. This indicates that the second phase and eutectic structure appear in the weld zone and precipitate aggregates at the grain boundaries. Fig. 3b shows the backscattered electron micrographs of the BM zone. The second phase particles Al_2Cu are found to be uniformly distributed in the base metal and do not aggregate at the grain boundaries [2].

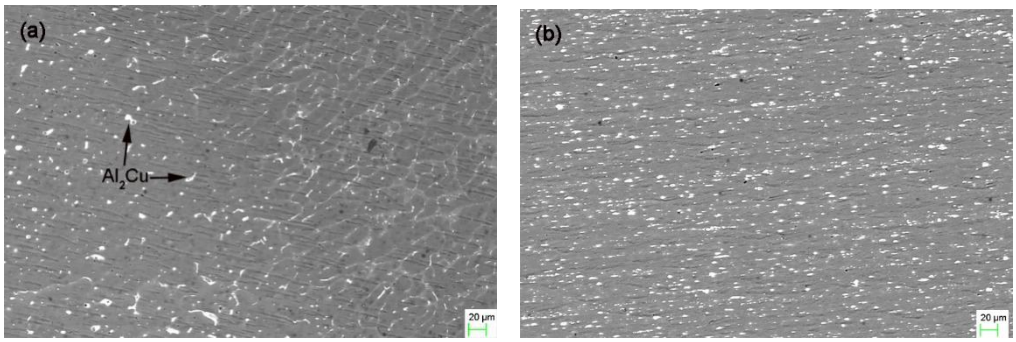

Figure 3. SEM images of AlCuRE welded joint: (a) welded joint near the FL, (b) BM zone.

Fig.4 shows the EDS mapping of Cu and Si element near the FL in AlCuRE welded joint. It can be found that the content of Si in the WZ is significantly higher than that in the HAZ, as shown in Fig.4b. Both Si and Cu are found in the WZ. The more closer to the FL, the higher the copper content. Therefore, both the Al-Si eutectic phase and the Al_2Cu phase precipitated at the grain boundaries of the columnar crystals.

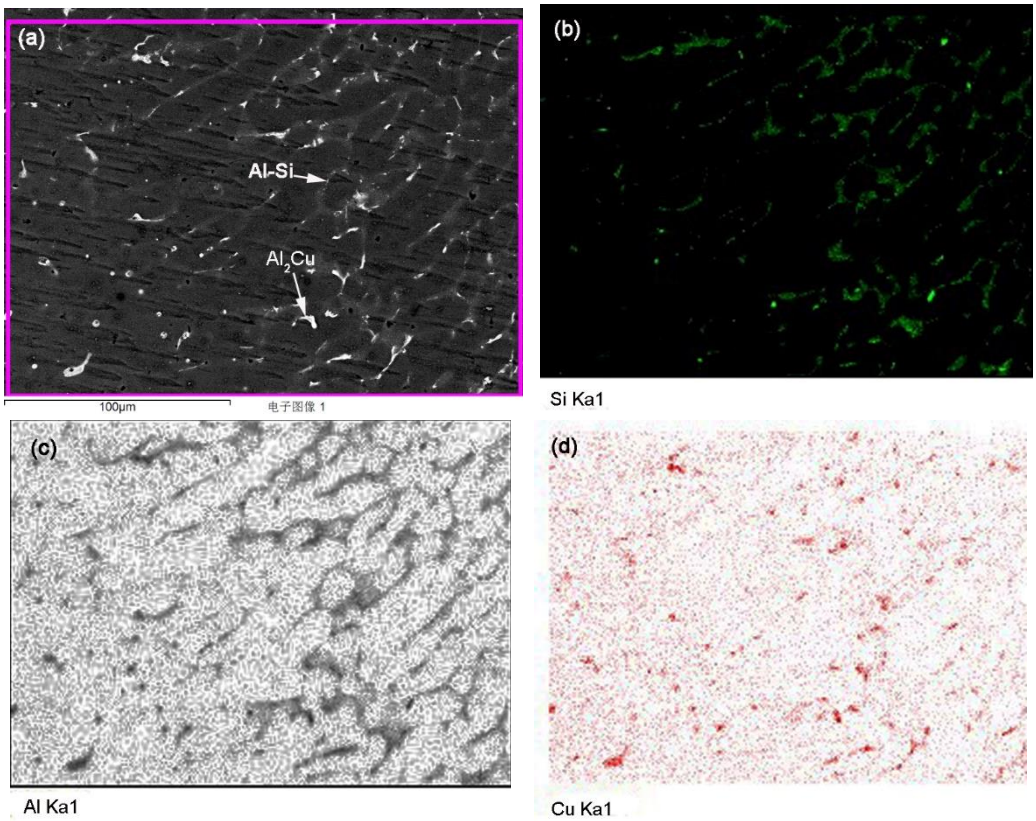

Figure 4. EDS mapping of Cu and Si element of AlCuRE welded joint near the FL.

3.2. Corrosion behavior

3.2.1 Potentiodynamic polarization plots

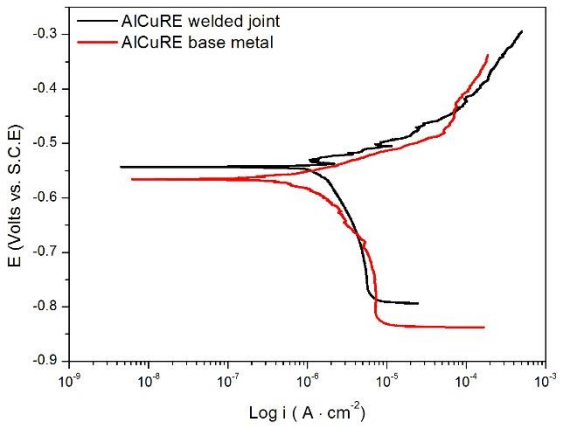

Figure 5. Potentiodynamic polarization plots of matrix and welded joint of AlCuRE alloy in alkaline soil extract.

Fig. 5 shows the potentiodynamic polarization curves of base metal and welded joint of AlCuRE alloy in liquid soil extract. The anode polarization curve of the base metal is smoother than that of the

welded joint. The anodic polarization curve of the welded joint appears zigzag, which indicates that pitting corrosion takes place in the polarization process again and again. The corrosion current densities (i_{corr}) of base metal and welded joint are 1.071×10^{-6} A/cm^2 and 3.355×10^{-6} A/cm^2, respectively, as shown in Table 4. The corrosion rate of welded joint is three times higher than that of base metal.

Table 4. The electrochemical parameters obtained from potentiodynamic polarization curves

	corrosion current (A/cm^2)	corrosion potential(mV/SCE)
AlCuRE base metal	1.071×10^{-6}	-565
AlCuRE welded joint	3.355×10^{-6}	-543

3.2.2. EIS Measurements

EIS results of the base metal and the welded joint in liquid alkaline soil extract are shown in Fig. 6. There was one time constants in the tested frequency interval for all EIS results which identifying one maximum in phase angle plots, as shown in Fig. 6a. Similarly, only one capacitive circle can be found for all EIS plots as shown in the Fig. 6b. The impedance modulus of the welded joint is significantly lower than that of the base metal, which indicated that the corrosion resistance of the welded joint is worse than that of the base metal.

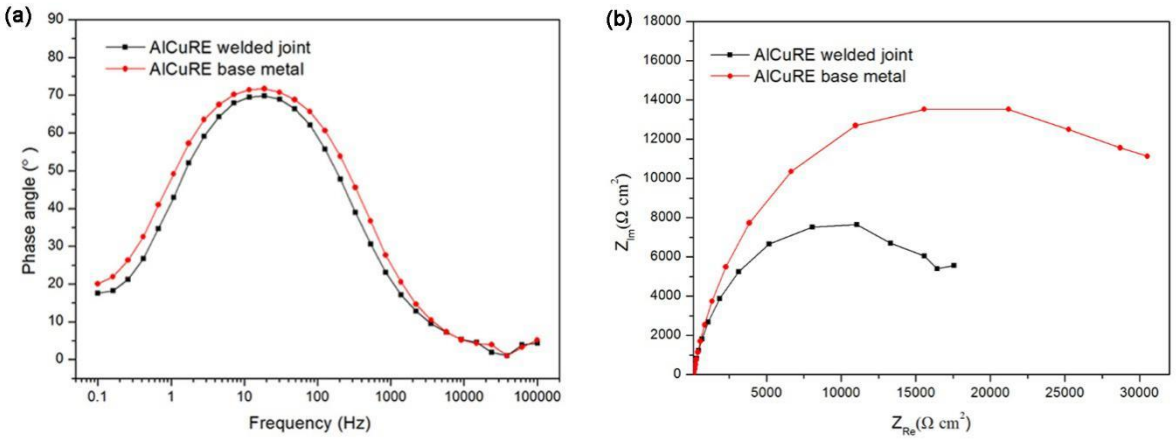

Figure 6. Nyquist and bode plots of matrix and welded joint of AlCuRE alloy in alkaline soil extract: (a) Bode diagram; (b) Nyquist diagram.

The corrosion electrochemical reactions can be analyzed by using EIS results. A model had been selected to calculate the kinetic parameters as shown in Fig. 7. The equivalent circuit is a series connection of the solution resistance R_s and one time constants QR_t. It was found that the $R_s(QR_t)$ elements can fit sensationally the experimental data, indicating a reasonable modeling. The impedance parameters calculated by the modeling are listed in Table 5. R_t represents the charge transfer resistance

and Q represents double-layer capacitance. R_t is an effective criterion to evaluate the corrosion speed of metal in corrosion system. The smaller the value of the R_t, the easier the charge transfer. It is observed that the R_t value of welded joint is smaller than that of matrix, indicating a more susceptible to corrosion of welded joint in alkaline soil extract.

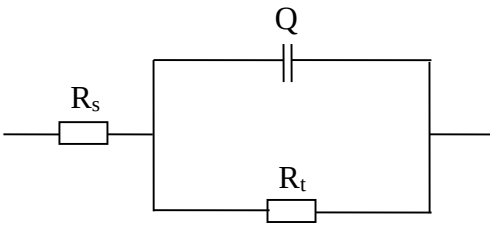

Figure 7. Circuit model of AlCuRE alloy in liquid alkaline soil extract.

Table 5. Fitted EIS results for Al alloy samples measured in soil extract.

Sample	$R_s/\Omega cm^2$	$Q/\Omega^{-1}cm^{-2}s\text{-}^n$	n	$R_t/\Omega cm^2$
Welded joint	102.9	1.309×10^{-5}	0.8524	1.955×10^{4}
Matrix	109.1	9.464×10^{-6}	0.8556	3.558×10^{4}

3.2.3. Potential distribution

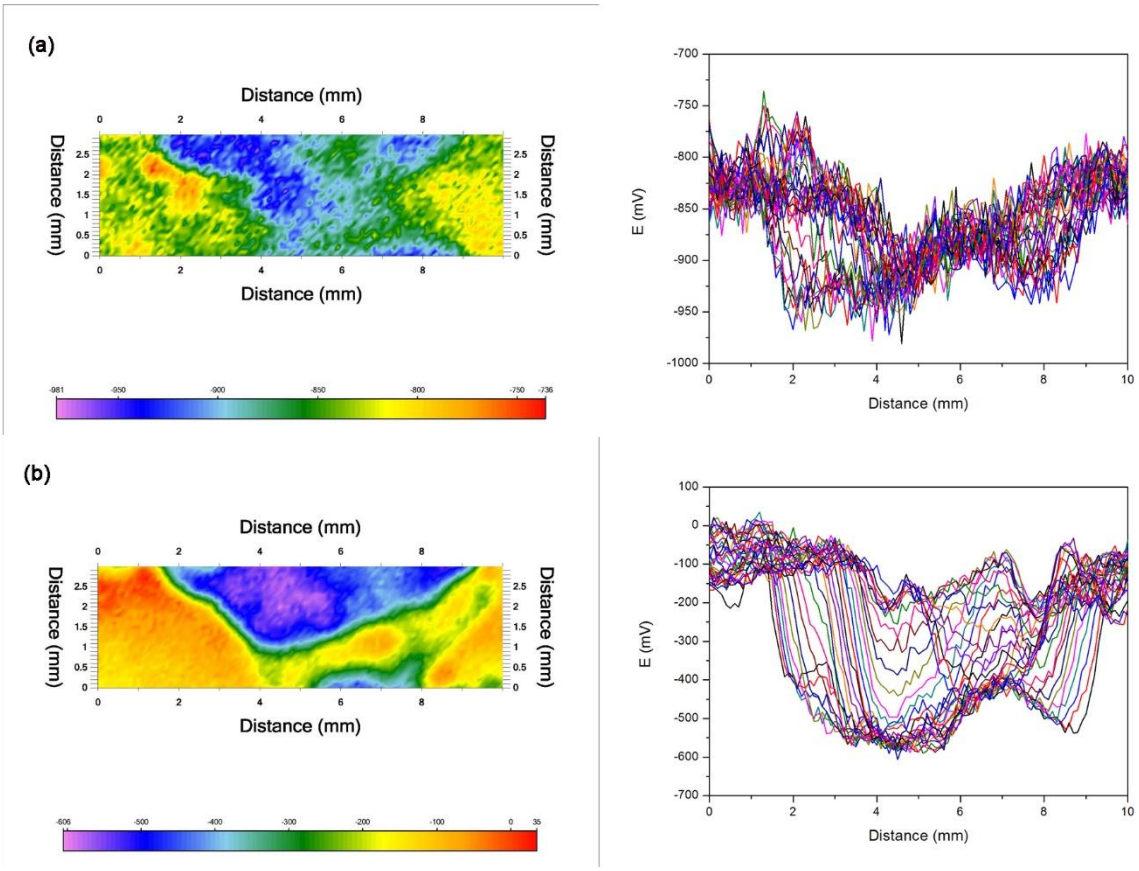

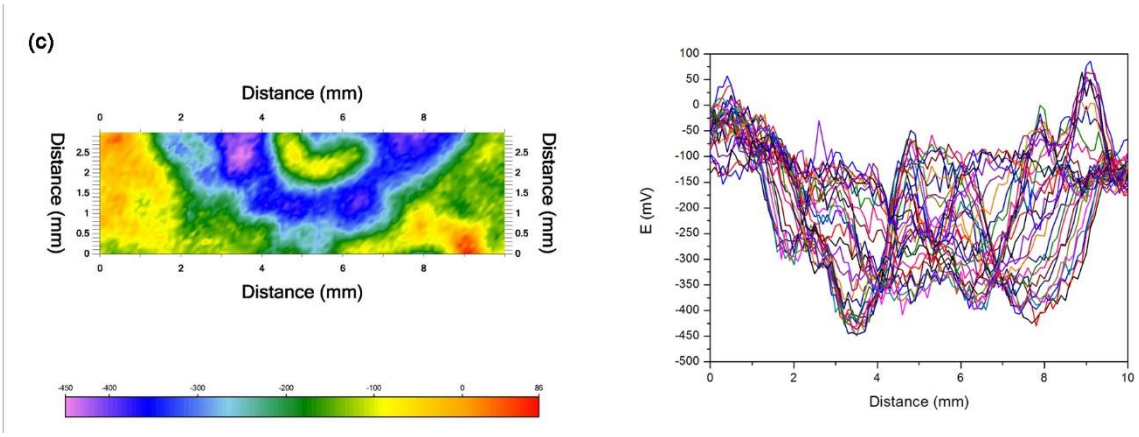

Figure 8. Surface potential distribution obtained by SKP for welded joint of AlCuRE alloy after different immersing time: (a) 0h, (b) 40h, (c)90h

As shown in Fig. 8, the surface potential of WZ is always lower than that of HAZ in different stages of immersion test. With the increase of immersion time, the potential difference between HAZ and WZ increases from 200mV to 600mV and then decreases to 550mV. However, the surface potential of welded joint is increasing with the immersion time.

When the welded joints are immersed in liquid alkaline soil extract, not only micro-electrochemical corrosion happens but also macro-galvanic corrosion is caused by potential difference between WZ and HAZ. The corrosion type of welded joint is oxygen absorption corrosion due to the alkaline corrosion medium [24,25]. Micro-electrochemical corrosion is the oxidation reaction of metal. Macro-galvanic corrosion is the dissolution reaction of metal in anode area. In the welded joint, since the potential of the WZ is low, so the WZ as an anode appears the dissolution reaction of Al. The HAZ was protected as a cathode. Therefore, the formation rate of oxide film and corrosion products in the WZ is much lower than that in the HAZ, resulting in the increase of potential difference.

3.2.4. Corrosion products

Figure 9 shows the effect of immersing times on surface three-dimensional corrosion morphology of MIG welded AlCuRE alloy joint in the soil extract measured by optical profilometer. The corrosion morphology of WZ with 60h immersing is shown in Figure 10. It is obvious that pitting mainly occurs near the FL. The diameters of pits vary from 0.01mm to 0.5mm and the depths of pits vary from several microns to dozens of microns, which can be seen from Figure 10. In the process of immersion test, some pits expand and grow up, and some pits disappear. The disappearance of pitting pits is caused by two factors. On the one hand, the initial state of pitting is metastable, and then it is passivated again [26-28]. On the other hand, some pitting pits are filled with corrosion products in the immersion test. At the beginning of the test, the roughness of the WZ is obviously larger than that of the HAZ. However, after immersing for 90 hours, the roughness of the HAZ increases obviously. The increase of the roughness of the HAZ is mainly due to the adsorption of soil particles on the sample

surface, which is confirmed by SEM. However, no soil particles are adsorbed on the surface of the WZ due to the dissolution reaction of metal.

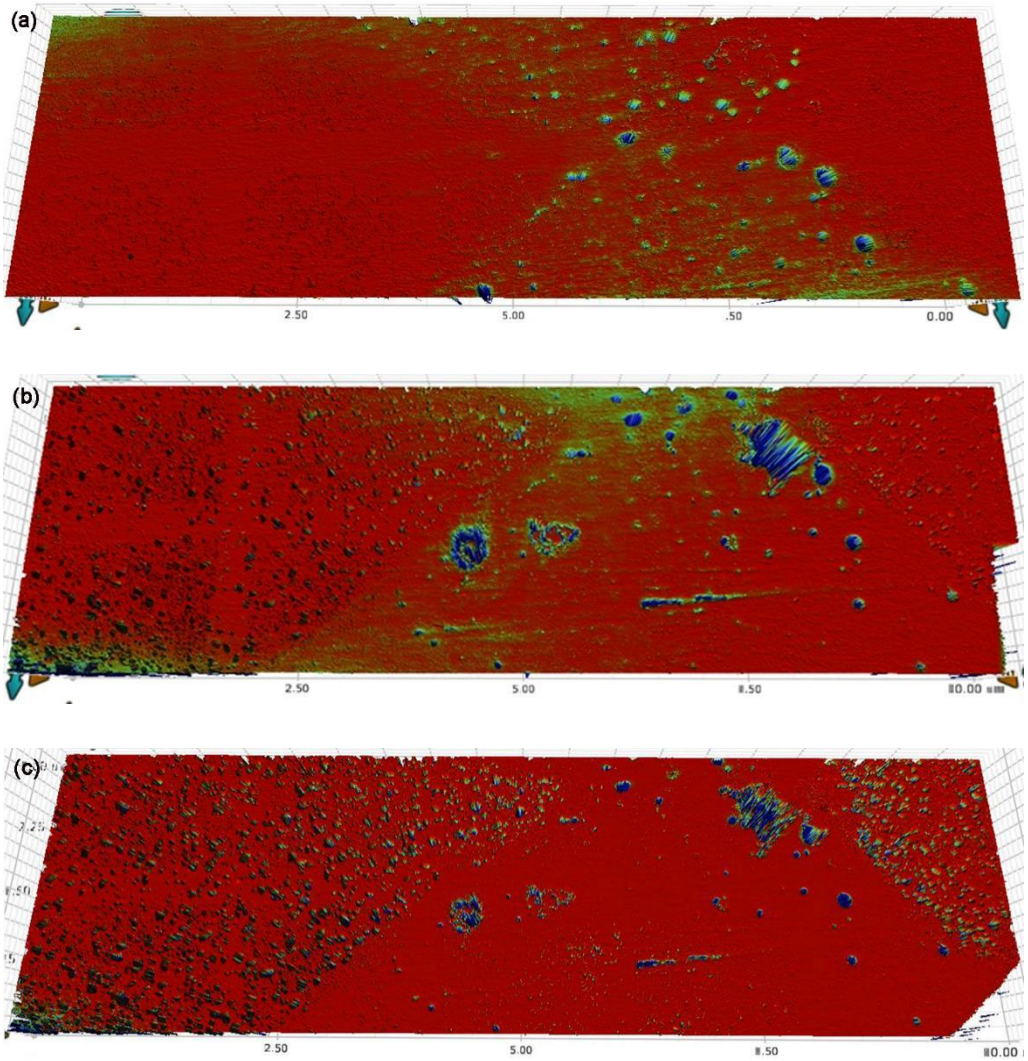

Figure 9. 3D corrosion morphology of MIG welded AlCuRE alloy joint measured by optical profilometer after immersing different time: (a) 20h, (b) 90h, (c) 150h.

Figure 11 shows the corrosion morphology of different zone of AlCuRE alloy welded joint after immersing for 150h. The image shows that both local corrosion and pitting corrosion occur in the WZ. The pitting corrosion is mainly concentrated in the columnar crystal zone near the FL. The surface of the WZ is covered with corrosion products, and the corrosion products are cracked and peeled locally. No obvious corrosion products can be found on the HAZ. But the surface of the HAZ absorbs a large number of soil particles in the soil extract, which result in uneven surface.

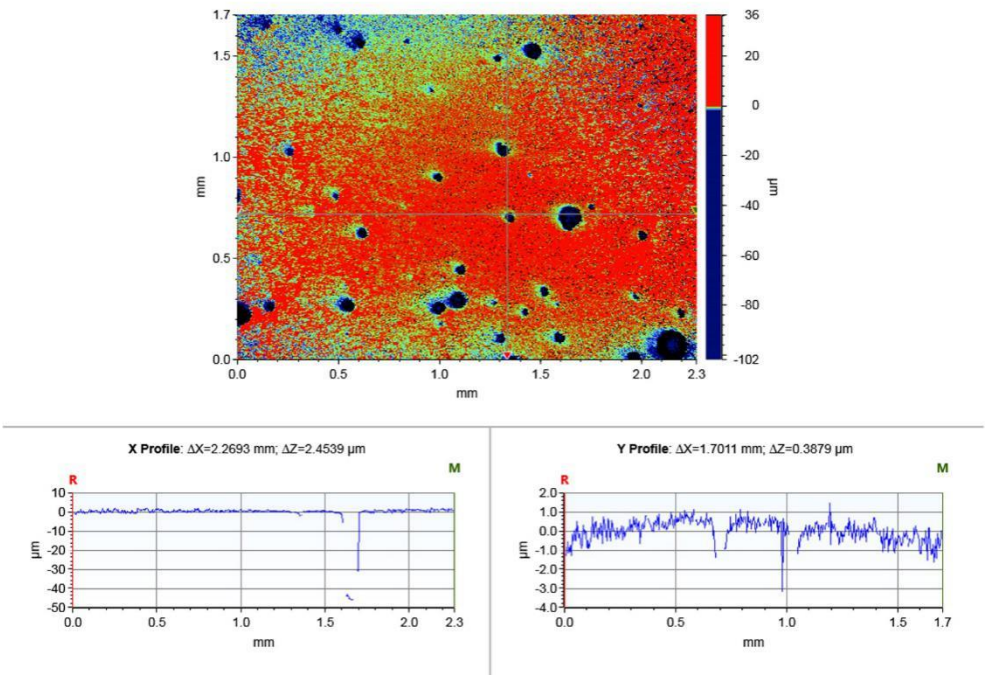

Figure 10. Corrosion morphology of WZ of AlCuRE alloy measured by optical profilometer after immersing 60h

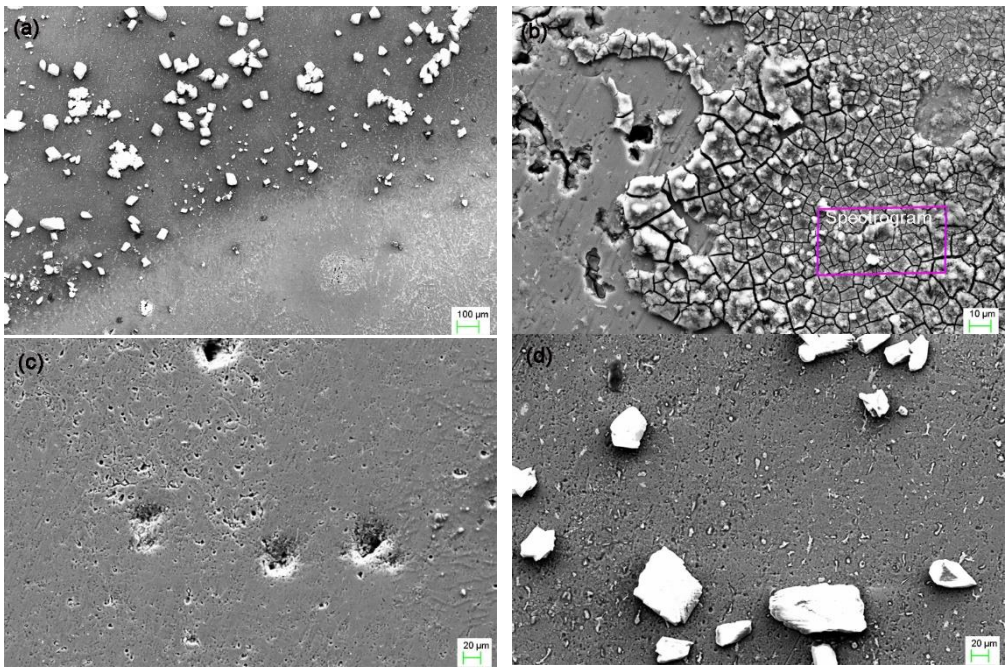

Figure 11. Microscopic corrosion appearance of different zone of AlCuRE alloy welded joint after being immersed for 150h: (a) fusion zone 50X, (b) WZ 500X, (c) WZ 200X, (d) HAZ 200X.

Figure 12 shows the EDS spectrum of corrosion products in WZ after 150h immersion. The EDS test zone is shown in Figure 11b. The composition of the corrosion products was 35.04Al, 46.33O, 1.53Si, 0.8S, 0.10Cu and 16.15C. The welded joint of AlCuRE alloy takes place oxygen absorption

reaction in alkaline soil extract, the anode reaction is aluminum electron loss process, the cathode is oxygen reduction reaction, so the corrosion products are mainly aluminum oxide. The contents of chloride ion(Cl^-) and sulfate ions (SO_4^{2-}) are high in the corrosion medium as shown in Table 3. Under the action of chloride ion, the oxide film of the WZ of AlCuRE alloy is destroyed, the corrosive anion reacts with the metal substrate, causing pitting corrosion [29], and the sulfide of aluminum is formed. So the corrosion products of welded joint of AlCuRE alloy in alkaline soil extract are mainly aluminum oxides and sulfides.

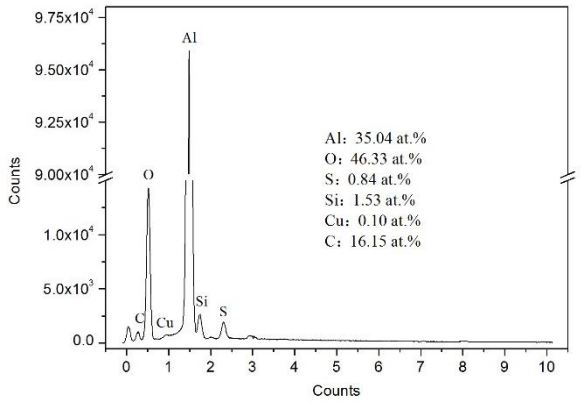

Figure 12. EDS spectrum of corrosion products in WZ after AlCuRE alloy joint was immersed for 150h.

3.3. Disccusion

Chloride ion can react with the base metal by not only destroying the surface oxide film, but also permeating the thin oxide film. This is one of the most corrosive anions [2]. Chloride ion can induce pitting on metal surface and sulfate ion can enlarge the area of pitting, resulting in metastable pitting change to steady pitting [30]. The high content of chloride ion and sulfate ion in corrosion medium is one of the reasons for the corrosion of welded joints.

The predominant second phases in WZ of AlCuRE alloy joint are Al_2Cu and Al-Si eutectic phase. And the precipitated second phase gathers at the grain boundary. Some studies mentioned that the precipitation of the second phase in the welded joint can accelerate the corrosion[3,19]. The electrode potential of Al-Si eutectic phase is similar to that of aluminum matrix, which has little effect on the corrosion of welded joints. However, the electrode potential of Al_2Cu phase is higher than that of the aluminum base metal. The aluminum matrix near the Al_2Cu particles dissolves preferentially as anode[7,19]. Since the Al_2Cu phase is mainly distributed in the columnar crystal boundary near the FL, so pitting mainly occurs in the columnar crystal zone.

The difference of the microstructure and composition of the welded joint leads to the difference of the surface potential and the macro galvanic corrosion of the welded joint. When the welded joint is immersed into alkaline soil extract, the metal of WZ as anode takes place metal dissolution reaction, while the HAZ as cathode occurs oxygen absorption. This is the main cause of WZ corrosion.

The corrosion of WZ is mainly caused by three aspects. One is the macro galvanic corrosion caused by the difference of surface potential between the HZA and WZ. The second aspect is micro

galvanic corrosion caused by the potential difference between the second phase and the base metal. The third aspect is the redox reaction of the WZ. Under the combined action of the three factors, the WZ corrosion takes place priority.

5. CONCLUSIONS

In this study, the corrosion behavior of MIG welded AlCuRE alloy joint in alkaline soil extract were studied by immersion corrosion test and electrochemical test, and the main conclusions are as follows.

(1) The microstructure of the WZ is as-cast structure with equiaxed dendrite in the central zoneof WZ and the columnar crystal near the FL.

(2) According to Potentiodynamic polarization curve and impedance spectrum, the BM has the higher corrosion resistance than MIG welded joint in alkaline soil extract.

(3) The surface potential of the WZ is obviously lower than that of the HAZ. The potential difference between the WZ and the HAZ increases firstly and then decreases slightly when the welded joints were immersed in the alkaline soil extract. The surface potential raised with immersion time.

(4) The corrosion behaviors of welded joint in alkaline soil extract are mainly pitting corrosion and local peeling corrosion. The corrosion resistance of WZ is the worst with pitting in the columnar crystal zone near the FZ and the corrosion products of aluminum oxides and sulfides.

(5) The corrosion of WZ is mainly caused by the difference of surface potential which is caused firstly by the differences of chemical composition and microstructure of welded joints and secondly by the distribution of second phase.

ACKNOWLEDGEMENTS
This work is supported by State Grid Shandong Electric Power Research Institute of China (No. 2016-62).

References

1. M. Fu, F.J. Yan, J. Yong, X.G. Li, Z.W. Yue and X.G. Wang, *Electric Power*, 48 (2015) 100.
2. F.J. Yan, X.G. Wang, X.M. Wang, X.G. Li and C.G. Wang, *International Journal of Electrochemical Science*, 12 (2017) 11212.
3. S.F. Zhang, Y. F. Hao, X.M. Wang, H. Chen, X.Y. Liao, M.X. Li, *Transactions of the china welding institution*, 38 (2017) 22.
4. D. Zhang, W.H. Chen, C.G. Wang, F.B. Dong, *Corrosion & protection*, 33 (2012) 705.
5. W.F Xu, J.H. Liu, H.Q Zhu, *Electrochimica Acta* 55 (2010) 2918.
6. J. Kang, R.D. Fu, G.H. Luan, C.L. Dong, M. He, *Corrosion science*, 52 (2010) 620.
7. W.F. Xu, J.H. Liu, *Corrosion science* 51 (2009) 2743.
8. A. Squillace, A. De Fenzo, G. Giorleo, F. Bellucci, *Journal of materials processing technology*, 152 (2004) 97.
9. M. Jariyaboon, A.J. Davenport, R. Ambat, B.J. Connolly, S.W. Williams and D.A. Price, *Corrosion Science*, 49 (2007) 877.
10. J. Kang, Z.C. Feng, G.S. Frankel, J.C. Li, G.S. Zou and A.P. Wu, *Corrosion*, 72 (2016) 719.
11. X.J. Wang, X.L. Wei, J.Y. Zhang, W.B. Chen, *Material Protection*, 50 (2017) 13.

12. J. Kang, Z.C. Feng, J.C. Li, G.S. Frankel, G.Q. Wang and A.P. Wu, *Metallurgical and materials Transactions A*, 47 (2016) 4566.
13. C.S. Paglia, R.G. Buchheit, *Materials Science and Engineering A*, 429(2006)107.
14. A. Venugopal, K. Sreekumar, and V.S. Raja, Metallurgical and materials transactions A, 41 (2010) 3151.
15. Z.Y. Zhu, C.Y. Deng, Y. Wang, Z.W. Yang, J.K. Ding, D.P. Wang, *Materials and Design*, 65 (2015) 1075.
16. Y.T. Lin, D.P. Wang, M.C. Wang, Y. Zhang and Y.Z. He, *Science and Technology of Welding and Joining*, 21 (2016) 234.
17. X.Y. Liao, Y.F. Hao, S.F. Zhang, X.M. Wang, Y.L. He, M.X. Li, *Corrosion and protection*, 37 (2016) 618.
18. Q. Li, A.P. Wu, Y.J. Li, G.Q. Wang, D.Y. Yan and J. Liu, Material Science & Engineering A, 623 (2015) 38.
19. H. Zhang, D.T. Sun, H. Zhang, F.F. Ma, J.H. Huang, *Rare metal materials and engineering*, 44(2015)103.
20. H. Zhang, D.T. Sun, H. Zhang, Y.H. Zhao, F.F. Ma, K.R. Xu, *Journal of chinese society for corrosion and protection*, 33 (2013) 175.
21. S.H. Yan, H. Chen, C.P. Ma, Y. Yuan, X.M. Wang and Q.H. Qin, *Materials and Design,* 88 (2015) 1353.
22. S.R. Koteswara Rao, G. Madhusudhan Reddy, K. Srinivasa Rao, M.Kamaraj, K. Prasad Rao, *Materials Characterization*, 55 (2005) 345.
23. G.Q. Gou, N. Huang, H. Chen, D. Li, L.C. Meng, *Transactions of the china welding institution*, 32 (2011) 17.
24. K. Li, *Oil-gas field surface engineering*, 32 (2013) 118.
25. T. Huang, X.P. Chen, X.D. Wang, F.Y. Mi, R. Liu, X.Y. Li, *Journal of Chinese Society for Corrosion and Protection*, 36 (2016) 31.
26. B.W. Davis, P.J. Moran, P.M. Natishan, *Corrosion Science*, 42 (2000) 2187.
27. G.S. Frankel, *Journal of the Electrochemical Society*, 145 (1998) 2186.
28. O. Lensch, B. Enders, J. Knecht, W. Ensinger, *Nuclear Instruments and Methods in Physics Research B*, 175-177 (2001) 683.
29. F.J. Yan, X.G. Li, B. Jiang, Z.B. Fan, S.L. Tian, *Corrosion science and protection technology*, 31(2019) 155.
30. A.J. Yan, R. Li, W.R. Song, B. Deng, L. Liu, D. Jiang, M. Cao, *Corrosion & protection*, 33 (2012 Suppl 2) 159